NUMERICAL ASSESSMENT OF ADDED RESISTANCE IN WAVES OF THE DTC CONTAINER SHIP IN FINITE WATER DEPTHS

Ivana Martić, Faculty of Mechanical Engineering and Naval Architecture, University of Zagreb, Croatia
Guillermo Chillcce Institute of Ship Technology, Ocean Engineering and Transport Systems (ISMT), the University of Duisburg-Essen, Germany
Manases Tello Ruiz, Maritime Technology Division, Ghent University, Belgium
Jorge Ramirez, Knud e Hansen A/S, Denmark
Nastia Degiuli, Faculty of Mechanical Engineering and Naval Architecture, University of Zagreb, Croatia
Bettar Ould el Moctar, Institute of Ship Technology, Ocean Engineering and Transport Systems, the University of Duisburg-Essen, Germany

SUMMARY

In this study, added resistance in waves of DTC container ship at full draft is investigated by means of Reynolds Averaged Navier-Stokes (RANS) solver in finite water depths. Validation is conducted against the experimental results of tests carried out with a scale model of DTC in the Towing Tank for Manoeuvres in Confined Water at Flanders Hydraulic Research (in co-operation with Ghent University and in the framework of the SHOPERA project). Following the numerical study of the ship resistance in calm water, the increase in resistance introduced by incoming waves for different advancing speeds is computed. This study shows the capabilities and reliability of RANS based methods to calculate the added resistance in finite water depth waves.

NOMENCLATURE

a_i	Face area vector (-)
a_0	Zeroth harmonic amplitude (-)
A_1	First harmonic amplitude (-)
A_2	Second harmonic amplitude (-)
B	Ship breadth (m)
C_{AW}	Added resistance coefficient (-)
C_ε	Turbulence model coefficient (-)
C_μ	Turbulence model coefficient (-)
f	Frequency (1/s)
f_c	Curvature correction factor (-)
Fr	Froude number (-)
$\overline{F}_x$	Average longitudinal force (N)
g	Gravitational acceleration constant (m^2/s)
G_k	Turbulent production term (kg/ms^3)
G_b	Production term due to buoyancy (kg/ms^3)
h	Water depth (m)
H_{max}	Fourier series maximum value (-)
H_W	Wave height (m)
k	Turbulent kinetic energy (m^2/s^2)
L_{PP}	Ship length between perpendicular (m)
P	Pressure (N/m^2)
$\overline{p}$	Mean pressure (N/m^2)
R_{AW}	Added resistance in waves (N)
R_F	Frictional resistance (N)
R_P	Pressure resistance (N)
R_T	Calm water resistance (N)
S_ε	User specified source term (kg/ms^4)
S_k	User specified source term (kg/ms^3)
T_e	Encounter period (s)
T_W	Wave period (s)
u_i	Velocity vector (m/s)
$\overline{u}_i$	Average components of the velocity vector (m/s)
u_{gi}	Grid velocity vector (m/s)
v	Velocity (m/s)
V	Cell volume (m^3)
$y+$	Non-dimensional wall distance (-)
α	Volume fraction of fluid (-)
ε	Turbulent dissipation rate (m^2/s^3)
ε_0	Ambient turbulence value (m^2/s^3)
ζ_A	Wave amplitude (m)
λ	Wave length (m)
μ	Dynamic viscosity (Pas)
μ_t	Eddy viscosity (kg/ms)
ν	Kinematic viscosity (m^2/s)
ρ	Density of water (kg/m^3)
σ_k	Turbulent Schmidt number (-)
σ_ε	Turbulent Schmidt number (-)
$\overline{\tau}_{ij}$	Mean viscous stress tensor (N/m^2)
Υ_M	Dilatation dissipation (m^2/s^3)

1 INTRODUCTION

The prediction of the ship added resistance in waves has increased in importance since the emission of harmful gases has been subjected to more stringent regulations via the Energy Efficiency Design Index (EEDI) (IMO MEPC.203(62), 2011). Added resistance in waves is understood as an increase in the required power to attain in waves a ship speed equal to the one in calm water, which in turn means more fuel consumption and therefore an increase in the amount of air pollutants emission.

An accurate prediction of attainable ship speeds when sailing in waves is then essential to assess the ship's performance in operating conditions and to determine the ship's impact on the environment. In literature, one can find that most studies have been conducted in open seas, see e.g. Sigmund and el Moctar (2018), Kim et al., (2017), Riesner and el Moctar (2018), Yasukawa and Adnan, (2006) and Chen et al. (2018). The study of the added resistance in waves in finite water depths should also be carried out. This is relevant when ship sails in finite water depths in close proximity of densely populated areas, when approaching or leaving a port, where restrictions on pollutants emissions are even more stringent.

The influence of waves on the sailing ship in finite depths has been investigated by few authors, for instance in Vantorre and Journée (2003), Tello Ruiz et al. (2015) and Tello Ruiz et al. (2016 and 2019). In Vantorre and Journée (2003) the analysis is focused on the ship motions of a container ship, a tanker and a bulk carrier. Experimental results were compared against numerical results obtained with 2D strip theory (Octopus Seaway). The comparison showed a fair agreement for wave lengths close to the ship length. For shorter waves, the discrepancy between the results was observed to be larger but still remained a good approximation. In Tello Ruiz et al. (2015) KVLCC2 at model scale has been investigated in regular waves, at different under keel clearances (UKCs), and different ship speeds. The test results for ship motions and wave forces (including the mean second order wave forces) were compared with numerical results obtained with three different potential codes (WAMIT for the zero speed case, HydroStar and Octopus Seaway). The numerical results obtained with all three potential codes showed a fair agreement with the experimental values for the ship motions, but none of them predicted the wave forces with a sufficient accuraccy. In Tello Ruiz et al. (2016 and 2019) similar results were obtained for ship motions and wave induced forces when the results of model tests, conducted with an ultra large container ship (ULCS), were compared against the numerical results obtained with HydroStar.

Potential methods, especially at forward speed, do not accurately deal with the interaction of the steady and unsteady oscillatory wave system. Such interaction will be even stronger in shallow water, thus the suitability of potential methods for the shallow water problems is questionable. As pointed out in Chen et al., (2018) the proximity of the bottom will increase the relevance of viscous effects and their influence on the ship motions and ship behaviour in general.

Reynolds-Averaged Navier Stokes (RANS) methods are a very good alternative to potential methods as they account for viscous effects in the numerical calculations. In that way, they can provide a better insight into the fluid phenomena for the shallow water problems. In literature, one can find a fair amount of studies where Computational Fluid Dynamics (CFD), based on the viscous flow theory, has been used in finite water depths, but most of them are either conducted in calm water (e.g. Toxopeus et al., 2013; Liu et al., 2017; Van Hoydonck et al., 2018) or at zero forward speed (e.g. Tezdogan et al., 2016). Only in Tello Ruiz et al. (2017), an ULCS sailing in waves at shallow water conditions has been studied with main focus on the interaction effects between the ship and the tank sidewalls, but no specific attention was drawn to the motions or forces, nor were the results validated.

In order to calculate ship added resistance in waves accurately, the prediction of ship motions is of great importance. In Tezdogan et al. (2015) an overset mesh was used to accommodate ship motions and the verification study showed small numerical uncertainties. This technique can accommodate large and arbitrary ship motions using overlapping technique. Besides its application for deep water cases (Carrica et al., 2007, Tezdogan et al., 2015), overset mesh has also been successfully used in confined water cases (Tezdogan et al., 2016) to calculate ship motions, and forces and moments acting on the ship hull. An alternative method to accommodate ship motions is the use of morphing mesh, which deforms locally around the ship hull as the ship moves. In Sigmund and el Moctar (2018) it has been successfully used for the calculations of ship motions and resistance in waves for both full and slender hull forms in deep water, and in Toxopeus et al. (2013) and Van Hoydonck et al. (2018) for the manoeuvring analysis in shallow water.

Even though it is generally assumed that the added resistance in waves is pressure driven and viscous effects are negligible, the viscous effects in short waves can increase in deep water, as shown in Sigmund and el Moctar (2018), and these effects should be investigated in finite water depths as well. When waves in shallow water start to be affected by proximity of the bottom, the orbital motion of fluid particles is disrupted, and water particles near the bottom flatten their orbit. As the water depth decreases, waves become steeper which will also have a noticeable influence on the added resistance (Chen et al., 2018).

To the authors' best knowledge, there are no specific studies dealing with the estimation of the added resistance due to waves in shallow and very shallow water. In this paper, this is numerically investigated for DTC container ship and validated against the experimental data. The experimental data are obtained from scale model tests conducted

in the Towing Tank for Manoeuvres in Confined Water at Flanders Hydraulic Research, within the framework of the European SHOPERA project (Van Zwijnsvoorde et al., 2019). The numerical calculations are performed with bare hull at 100% and 20% UKC, for two different speeds, with and without waves, Table 1.

2 SHIP GEOMETRY AND CONDITIONS

DTC (Duisburg Test Case) container ship was developed at the Institute of Ship Technology, Ocean Engineering and Transport Systems in Duisburg-Essen, Germany for benchmark purposes (see el Moctar et al., 2012). Captive and free running tests have been performed in the Towing Tank for Manoeuvres in Confined Water at Flanders Hydraulic Research (in co-operation with Ghent University) with a scaled model (1:89.11). A perspective view of the 3D model of DTC container ship is shown in Figure 1. Hull parameters and mass characteristics of the ship model can be found in Van Zwijnsvoorde et al., (2019). In this research, numerical simulations of captive model tests with the bare hull are performed in calm water and in regular waves, Table 1.

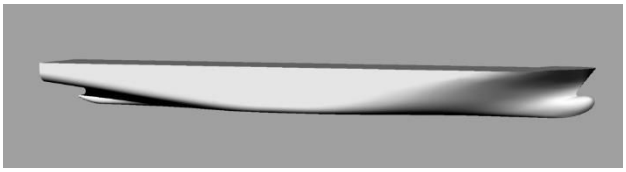

Figure 1. 3D model of DTC container ship.

Table 1. Test cases for numerical simulations

Test ID	Velocity, m/s	UKC, %	λ/L_{PP}	Wave height, mm	Wave period, s
C1	0.327	100	/	/	/
CW2	0.327	100	0.55	62.31	1.38
C3	0.327	20	/	/	/
CW5	0.327	20	0.55	21.26	1.66
C2	0.872	100	/	/	/
CW3	0.872	100	0.55	62.35	1.38

A post-processing analysis of the experimental data has been carried out for further comparison with the numerical estimations. The analysis was performed following the recommendations in Van Zwijnsvoorde et al., (2019) with respect to the selection of the time windows and adopting the approach described in Tello Ruiz et al. (2016) for harmonic signals. In this method, the signal is filtered with a band pass filter and further fitted with a least square method up to a third order Fourier expansion with eight unknown parameters, see equation (1).

$$f(t) = a_0 + \sum_{i=1}^{3} a_i \sin(i\omega t) + b_i \cos(i\omega t) \quad (1)$$

In Eq. (1) a_0 and ω are the mean and the frequency of harmonic signal, respectively; the remaining terms a_i, and b_i are the harmonic components related to the first, second and third order Fourier series. For the cases in calm water the analysis has been conducted over the same regions defined in the analysis selected for waves.

3 GOVERNING EQUATIONS

Numerical simulations of incompressible viscous flow around the ship hull are performed using the commercial software package STAR-CCM+. Navier Stokes equations and continuity equation are used for the description of the fluid motion. RANS equations and averaged continuity equation obtained by time averaging of Navier-Stokes equations and continuity equation are given as follows (Ferziger and Perić, 2012):

$$\frac{\partial(\rho\bar{u}_i)}{\partial t} + \frac{\partial}{\partial x_j}\left(\rho\bar{u}_i\bar{u}_j + \rho\overline{u_i'u_j'}\right) = -\frac{\partial\bar{p}}{\partial x_i} + \frac{\partial\bar{\tau}_{ij}}{\partial x_j} \quad (2)$$

$$\frac{\partial(\rho\bar{u}_i)}{\partial x_i} = 0 \quad (3)$$

where ρ is the fluid density, $\bar{u}_i$ is the averaged Cartesian components of the velocity vector, $\rho\overline{u_i'u_j'}$ is the Reynolds stress tensor, $\bar{p}$ is the mean pressure and $\bar{\tau}_{ij}$ is the mean viscous stress tensor defined as follows:

$$\bar{\tau}_{ij} = \mu\left(\frac{\partial\bar{u}_i}{\partial x_j} + \frac{\partial\bar{u}_j}{\partial x_i}\right) \quad (4)$$

where μ is the dynamic viscosity.

To close the system of equations (2) and (3), Realizable $k-\varepsilon$ (RKE) turbulence model is used as isotropic eddy-viscosity model based on the assumption that turbulence effects can be described as increased viscosity:

$$-\rho\overline{u_i'u_j'} = \mu_t\left(\frac{\partial\bar{u}_i}{\partial x_j} + \frac{\partial\bar{u}_j}{\partial x_i}\right) - \frac{2}{3}\rho\delta_{ij}k \quad (5)$$

where k is the turbulent kinetic energy defined as follows:

$$k = \frac{1}{2}\overline{u_i'u_j'} \quad (6)$$

The $k-\varepsilon$ turbulence model is commonly used in engineering applications providing good agreement with the experimental results while keeping the reasonable CPU time required to perform numerical simulations (Quérard et al., 2008).

Within $k-\varepsilon$ turbulence models, one equation is solved for turbulent kinetic energy k and one for turbulent dissipation rate ε, while eddy viscosity is described as follows:

$$\mu_t = \rho C_\mu \frac{k^2}{\varepsilon} \quad (7)$$

The transport equations for RKE are given as (CD-adapco, 2018):

$$\frac{\mathrm{d}}{\mathrm{d}t}\int_V \rho k \mathrm{d}V + \int_A \rho k(u_i - u_{gi})\cdot \mathrm{d}a_i = \int_A \left(\mu + \frac{\mu_t}{\sigma_k}\right)\frac{\partial k}{\partial x_i}\cdot \mathrm{d}a_i + \int_V \left[f_c G_k + G_b - \rho\left((\varepsilon - \varepsilon_0) + \Upsilon_M\right) + S_k\right]\mathrm{d}V \quad (8)$$

$$\frac{\mathrm{d}}{\mathrm{d}t}\int_V \rho \varepsilon \mathrm{d}V + \int_A \rho \varepsilon(u_i - u_{gi})\cdot \mathrm{d}a_i = \int_A \left(\mu + \frac{\mu_t}{\sigma_\varepsilon}\right)\frac{\partial \varepsilon}{\partial x_i}\cdot \mathrm{d}a_i + \int_V \left[f_c C_{\varepsilon 1} S\varepsilon + \frac{\varepsilon}{k}(C_{\varepsilon 1} C_{\varepsilon 3} G_b) - \frac{\varepsilon}{k+\sqrt{\nu\varepsilon}} C_{\varepsilon 2}\rho(\varepsilon - \varepsilon_0) + S_\varepsilon\right]\mathrm{d}V \quad (9)$$

where V is the cell volume, u_i is the velocity vector, u_{gi} is the grid velocity vector, a_i is the face area vector, σ_k and σ_ε are turbulent Schmidt numbers, f_c is the curvature correction factor, G_k is the turbulent production term, G_b is the production term due to the buoyancy, ε_0 is the ambient turbulence value in the source terms that counteracts turbulence decay, Υ_M is the dilatation dissipation, S_k and S_ε are user specified source terms, $C_{\varepsilon 1}$, $C_{\varepsilon 2}$ and $C_{\varepsilon 3}$ are model coefficients, S is the modulus of the mean strain rate tensor and ν is the kinematic viscosity.
The Volume of Fluid (VOF) method is used to capture the free surface between two phases in both calm water simulations and in waves, introducing the additional transport equation solved for the volume fraction:

$$\frac{\partial}{\partial t}\alpha + \nabla\cdot(\alpha u_i) = 0 \quad (10)$$

where the volume fraction of the phase in a computational cell α is 0 for air and 1 for water, and the value of 0.5 indicates the free surface. It enables modelling of two fluids as a single fluid whose physical characteristics calculated in each computational cell depend on the volume fraction of the phase in that particular cell, while the same governing equations as for a single-phase problem are being solved. The second order convection scheme is used to capture the interface between two phases. Segregated flow model is used to solve the flow equations in an uncoupled manner and SIMPLE algorithm is used for implicit coupling between the pressure and the velocity. Convection terms in RANS equations are discretized by second-order upwind scheme. RANS solver calculates forces acting on the ship hull based on the Dynamic Fluid Body Interaction (DFBI) model, which enables motions of the rigid body and re-positioning at each time step. It should be noted that only two degrees of freedom are activated for the ship, i.e. heave and pitch motion.

4 COMPUTATIONAL DOMAIN AND BOUNDARY CONDITIONS

Boundaries of the computational domain are all placed 1.2 L_{PP} away from the ship except for the bottom boundary. It should be noted that for the sake of reducing the computational time, only half of the domain is simulated and the symmetry condition is applied. Before running the simulation, initial and boundary conditions have to be defined, depending on the problem that is being solved. Velocity inlet is applied on the inlet and top boundary. For simulations in calm water, the velocity is equal to the ship velocity but in opposite direction and for simulations in waves the initial velocity is set to the corresponding velocity of the incoming waves. Side and bottom boundaries are set as non-slip wall condition, moving with velocity equal to ship velocity but in the opposite direction. The hull surface is also set as non-slip wall condition. The outlet boundary is set as the pressure outlet condition to fix static pressure at the outlet of the computational domain. As already mentioned, the symmetry condition is applied to the symmetry plane.

The problem is solved in an inertial coordinate system that travels along with the ship. In that way, the ship has zero forward speed and the fluid has a velocity equal to the ship speed but in opposite direction. In the case of simulations in waves, besides the characteristics of the incoming waves, at the inlet boundary the additional velocity is set to simulate the ship advancing in waves and to achieve the correct wave encounter frequency.

A mesh morphing algorithm is used to deform the numerical grid and accommodate ship motions in the computational domain. An unstructured grid is generated using hexahedral control volumes. Local grid refinements are used near the bow, stern and between the ship and the bottom boundary to properly capture the features of complex flow around the ship hull. A refinement where the free surface is expected is made to capture the ship's wake. The finest free surface refinement has a minimum of 100 cells per wave length and 20 cells per wave height. Mesh section for the 100% UKC case can be seen in Figure 2. To model the inner region of the boundary layer, all y+ wall treatment is used which consists of a hybrid treatment that emulates the low and high y+ treatment depending on the size of the cell near the wall (CD-adapco, 2018).

Six prism layers are used to resolve the boundary layer flow near the hull. The initial aim was to achieve y+ less than one, but this gave a numerical ventilation problem due to very thin cells near the wall. Therefore, all y+ value treatment was adopted. The numerical domain for the calm water simulations has about 7.1 million cells for C1 and C2, and 7 million cells for case C3. In the case of waves, CW2 and CW3 have up to 7.6 million cells while CW5 has 8.9 million cells. It should be noted that the same mesh could have been used for both simulations in calm water and in waves at certain ship speed. However, with the respect to the required computational time, the mesh for test cases in waves has been additionally refined near the free surface in the vertical direction in order to better capture the free surface elevation.

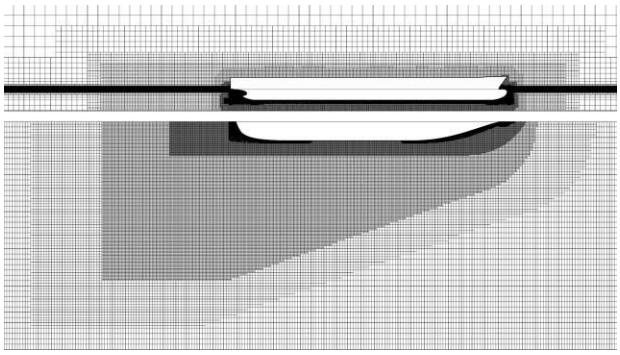

Figure 2. Mesh section for 100% UKC case.

To prevent wave reflection from the boundaries, for simulations in calm water, VOF wave damping is used at inlet, outlet and side boundaries. The damping length is set as a function of physical time, to speed up the convergence at the beginning of the simulation, reducing the size of the damping zone to 0.6 L_{PP} as the simulation advances. For simulations in waves, a forcing method is applied to prevent wave reflections from the boundaries. In this way, a significant reduction in the size of the computational domain is possible compared to the size of the domain that would have to be used if a wave damping method would be applied. Forcing is applied at inlet, outlet and side boundary as well, up to a distance of 2.4 m and it ensures that in that region the wave amplitude is equal to the amplitude of the incoming wave. Both damping and forcing methods use additional source terms in the momentum equations.

5 COMPUTATIONAL PROCEDURE

In order to generate regular incoming head waves a fifth-order Stokes wave was used. To monitor the elevation of the generated waves, a wave probe is placed in front of the ship. Note that the amplitude of the first harmonic obtained from the Fourier series fitting applied to the wave amplitude has been further used for the normalization of added resistance in waves.

In the unsteady simulations in waves, the time step is chosen such that the Courant number is lower than 0.4 and following the ITTC's recommendation to use at least 100 time steps per wave period (ITTC, 2014). In this research, the time step equal to 0.002 s is used for the CW2 and CW5 cases, and 0.0015 s for the CW3 case.
To analyse the unsteady time series of forces acting on the ship hull their Fourier series is used as well.

Added resistance in waves is thus calculated by subtracting the calm water resistance R_T from the zeroth-order harmonic amplitude of the Fourier series, i.e. the average longitudinal force $\overline{F}_x$. The added resistance coefficient is obtained as follows:

$$C_{AW} = \frac{\overline{F_x} - R_T}{\rho g \zeta_a^2 B^2 / L} \tag{11}$$

where ζ_A is the wave amplitude.

6 RESULTS

6.1 CALM WATER RESISTANCE

All numerical simulations in calm water are performed as unsteady simulations with time step equal to 0.02 s. Initially a larger time step, based on the time required for the flow to pass one ship length, is reduced for cases C1 and C3 due to the appearance of numerical ventilation. This occurs when air particles get into the boundary layer below the free surface, and it affects the calculation of the frictional part of the total resistance. In other words, shear stress calculated using the air characteristics instead of water characteristics decreases.

The comparison between the numerically and experimentally obtained results can be seen in Table 2. The numerical results are taken as the average values of the last 10 s of the time series. From the comparison it can be seen that the smallest relative deviation (RD of 6.84%) is obtained for the C1 case. A significant increase in pressure resistance is noticed between test cases C1 and C3. In the case of C3 (shallower water) the pressure resistance contribution is over 30% of the total resistance, which is approximately twice larger than in the case of C1. It appears that pressure resistance increases faster than frictional resistance and is more affected by the proximity of the bottom.

For case C2, large relative deviation in the total resistance is possibly obtained due to numerical ventilation that could be observed in the large part of the ship hull, which could have consequently led to an underestimation of the frictional resistance. It occurred despite the small values of Courant number and even though a second-order upwind scheme was used. It should be noted that the trim and sinkage are underestimated as well.

Table 2. Comparison of total resistance values obtained numerically and experimentally

Test ID	EXP, (N)	CFD, (N)	RD, (%)	R_F, (N)	R_P, (N)
C1	0.81	0.75	6.84	0.62	0.13
C3	1.11	0.99	10.33	0.67	0.32
C2	5.5	4.77	13.25	3.76	1.01

6.2 WAVE ELEVATION

Wave elevation has also been measured at the position of the wave probe WG4 during the experiment. It is located at 4.03 m in the positive *x* direction and 0.65 m in portside direction with respect to amidships. Time series of the wave elevation measured during the numerical simulation and the comparison with the experimental values for the CW5 can be seen in Figure 3. The 1st harmonic wave amplitude, obtained from Fourier series fitting based on the last 10 s of the time series, is equal to 10.71 mm which

overestimates the experimental value by approximately 12%, Table 3. The differences encountered indicate that the wave amplitude does not remain constant as waves propagate along the tank, considering that the amplitude of wave generated at the inlet boundary was based on WG2, located upwards the model during the experiment. This has also been observed in Tello Ruiz (2018), where a region along the tank has been defined at which waves remain approximately (within 5%) constant. These variations indicate that when testing numerical methods in shallow water a larger domain would be required to model such phenomenon, however, this was not possible at this stage considering the large computational power required. Note that theoretical ratio between the wave length and ship length is equal to 0.55 which classifies the generated waves as medium waves relative to the ship length, and they correspond to the intermediate water depth waves in the case of both water depths investigated.

Table 3. Harmonic decomposition of the computed and measured time series for wave elevation

CW5		H_{max}, (mm)	f, (1/s)	a0, (mm)	A1, (mm)	A2 (mm)
ζ_A	EXP	19.51	4.72	1.48	9.56	1.52
	CFD	21.78	4.72	0.82	10.71	1.54

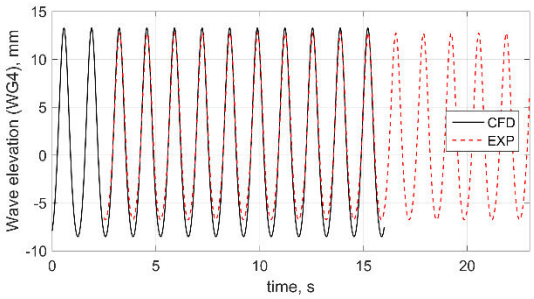

Figure 3. Time series of wave elevation at the position of wave probe WG4 for case CW5.

6.3 VALIDATION OF NUMERICAL SIMULATIONS IN WAVES

Validation of the numerical results for the simulations in waves is performed for the CW3 case, which corresponds to 100% UKC and model speed equal to 0.872 m/s. Numerical values obtained for the last eight encounter periods are taken to perform a Fourier fitting analysis. The computed longitudinal force in waves and its post-processed time series (obtained by applying the Fourier series up to the 3rd order) can be seen in Figure 4. The comparison with the post-processed experimental values is shown in Figure 5. The corresponding parameters obtained from the harmonic decomposition of the time series (the zeroth, the first and the second order harmonics) can be seen in Table 4. From Table 4 it can be observed that the mean value (the zeroth-order term) for the longitudinal force is equal to 7.71 N, which overestimates the experimental value by about 4.6%. In spite of the satisfactory agreement obtained, a numerical verification of the results is desired to exclude the grid and time step dependency of the numerical results.

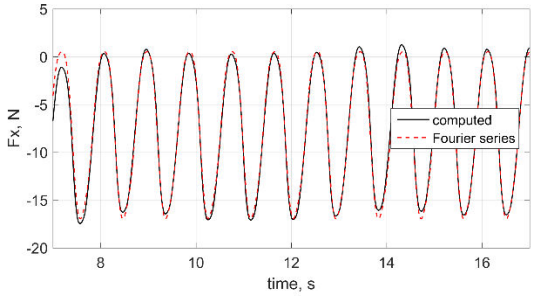

Figure 4. Fourier series approximation of the time series of longitudinal force for the CW3 case.

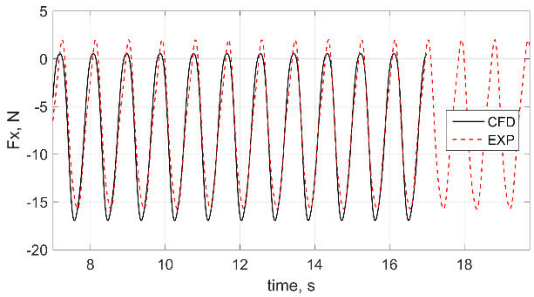

Figure 5. Comparison between numerical and experimental results obtained for the longitudinal force for the CW3 case.

Table 4. Harmonic decomposition of the computed and measured time series for the longitudinal force in waves

Test ID		H_{max}, (N)	f, (1/s)	a0, (N)	A1, (N)	A2 (N)
CW2	EXP	/	/	/	/	/
	CFD	17.00	5.48	-2.15	8.33	1.13
CW5	EXP	/	/	/	/	/
	CFD	6.94	4.71	-1.32	3.48	0.17
CW3	EXP	17.40	7.05	-7.37	8.55	0.90
	CFD	17.55	7.03	-7.72	9.08	0.74

6.4 RESULTS FOR 100% UKC

Time series of the longitudinal force for the CW2 case is shown in Figure 6. Again, the last eight encounter periods of the computed time series are used for the Fourier analysis. The magnitude of the zeroth-order harmonic of the Fourier series is equal to 2.15 N, which is a significant increase in in waves compared to the calm water resistance (0.75 N, see Table2). The orbital velocity of wave particles have a tendency to increase the shear stress and thus increase the frictional resistance in waves compared to the calm water case. For the CW2 case, the comparison shows that the frictional resistance has increased by about 20%, while for the CW3 case this increase is approximately 8%. From the results, it can be observed that there is a significant increase in the pressure resistance in waves for both cases. For the CW2 case, the mean value for pressure resistance accounts for 60 % of the total resistance in waves, which also leads to a significant increase in added resistance in waves. It is important to mention that in the

CW2 case numerical ventilation was also observed for a large portion of the hull wetted surface, especially in the fore part, see Figure 7. This was observed in the CW3 case as well, mostly in the front part of the hull. The transition between the air and water occurred over a large number of cells, resulting in a large number of cells having approximately the same volume fraction of air and water. This did not have a significant influence on the results for the test case CW3 unlike in the test case CW2 where large number of cells in the bow area have a volume fraction of water lower than 1 but higher than 0.5. The stronger numerical ventilation observed for the CW2 case causes an overestimation of the friction velocity, which is further used for the calculation of shear stress. Also, due to the high wave elevation at the bow part of hull, parts of the wave crests are captured by the coarser free surface refinement rather than the finest one.

The wave pattern around the DTC hull, at the end of the simulation, can be seen in Figures 8 and 9 for cases CW2 and CW3 respectively. The Kelvin wake is formed for both 100% UKC cases and is more emphasized for the test case conducted at the higher speed.

Table 5. Numerical and experimental values of the total resistance in waves

Test ID	EXP, (N)	CFD, (N)	$\overline{R_F}$, (N)	$\overline{R_P}$, (N)
CW2	/	2.15	0.75	1.40
CW5	/	1.32	0.75	0.57
CW3	7.37	7.71	4.06	3.65

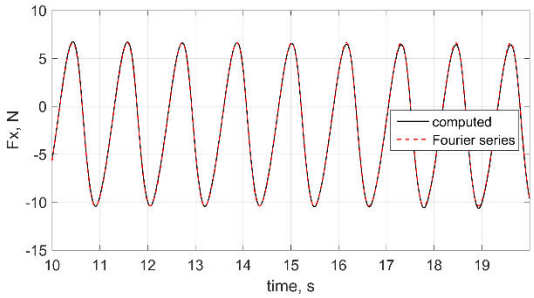

Figure 6. Time series of the computed longitudinal wave force for CW2.

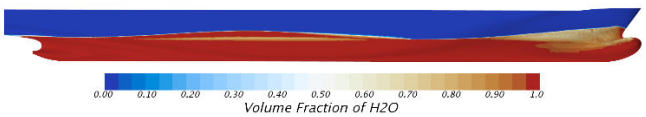

Figure 7. Free surface representation on the model hull for CW2.

In deep water where waves propagate freely, the group velocity is considered twice as small as the actual wave velocity. In shallow water, at large wave lengths, the group velocity and wave velocity are equal. If the ship velocity is smaller than the wave velocity, a Kelvin wake should be formed. However, in the case CW2 the system of divergent and transverse waves has not been fully developed.

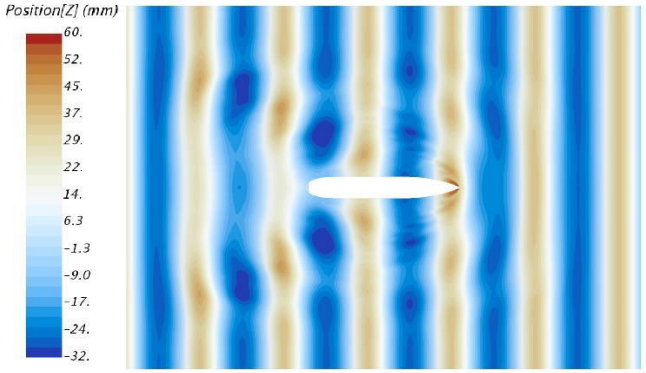

Figure 8. Free surface elevation for the test case CW2.

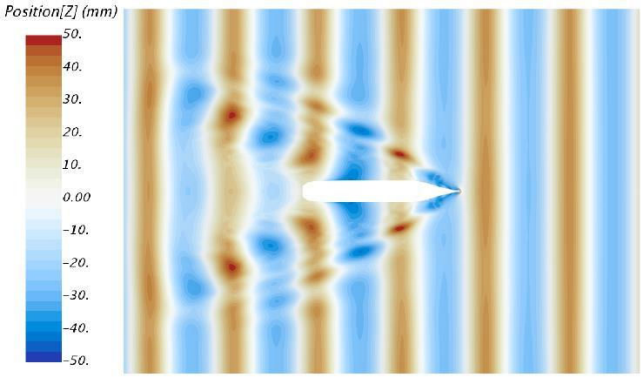

Figure 9. Free surface elevation for the test case CW3.

6.5 RESULTS FOR 20% UKC

In the test case CW5, which corresponds to 20% UKC at model speed equal to 0.327 m/s, the total resistance in waves is about 30% larger than the calm water resistance, Table 5. The frictional part has increased by about 11% compared to the calm water case. However, the frictional part of added resistance is about 24% of the total value. This is also common for relative short waves in deep water (Sigmund and el Moctar, 2018), where viscous effects are important and the corresponding increase in the frictional component of the added resistance in waves is larger than 20%.

Comparing the results with the similar test conditions with respect to waves and ship speed but different water depth (test case CW2 for 100% UKC) it can be observed that the mean value of frictional resistance remained almost the same, while pressure resistance increased by about 60%. However, taking into account the shortcomings that were observed in the numerical results for CW2, the numerical setup of that particular case should be improved in order to properly compare the results and draw valid conclusions.

For the CW2 and the CW5 cases a comparison of wall shear stress can be seen in Figure 10, and a comparison of the hydrodynamic pressure in Figure 11. Both hydrodynamic pressure and longitudinal shear stress in waves are presented at a time step corresponding to encounter period T_e.

Figure 10. Wall shear stress for the CW2 case (top) and the CW5 case (bottom).

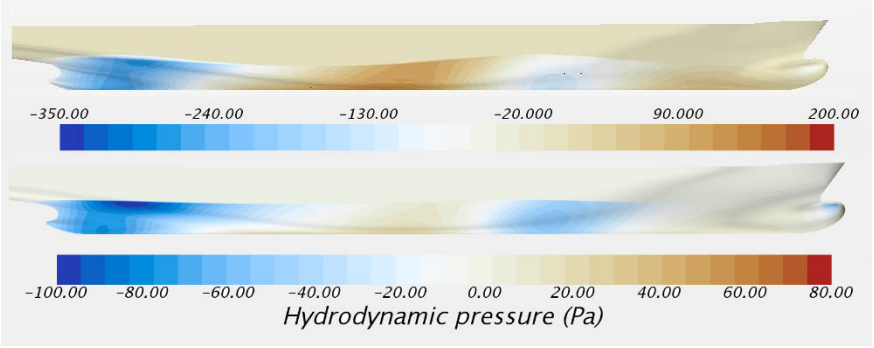

Figure 11. Hydrodynamic pressure on hull for the CW2 case (top) and the CW5 case (bottom).

The shear stress is larger for the CW2 case in the bow region due to the diffraction of the incident waves.

When it comes to hydrodynamic pressure, large differences can be observed. Pressure resistance consists of wave resistance and viscous pressure resistance, where the latter is in numerical sense very responsive to the numerical setup and different numerical disturbances, such as small pressure level changes during the simulation with larger numerical uncertainty compared to the frictional resistance (Raven et al., 2008). In the case of the CW5 results, it appears that very short waves are being reflected from the forcing zone at the side boundary, Figure 12. Parameters in the source term functions used to prevent wave reflections are dependent on wave characteristics and should be adjusted to the particular wave that is being forced. The same forcing coefficient is used for both CW2 and CW5, which possibly led to waves of approximately three times smaller elevation, in the case CW5, being reflected, Figure 12.

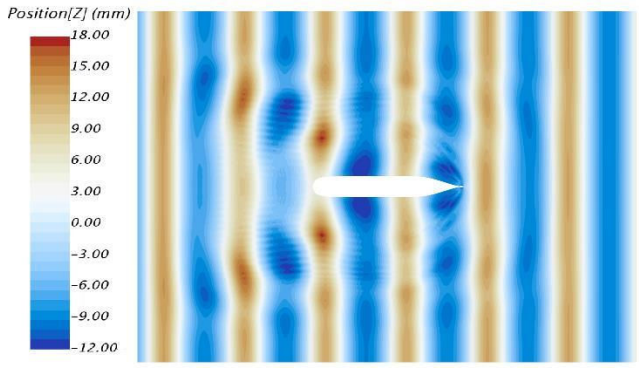

Figure 12. Free surface elevation for the CW5 case

In Table 6, the added resistance in waves for all tested cases can be seen along with the added resistance coefficient normalized using equation (11). As can be seen in the table, the largest added resistance coefficient is obtained for CW5 test case. Since added resistance in waves is very dependent on the ship speed, for the two comparable cases with the same wave characteristics, a larger added resistance coefficient is obtained for CW3 as expected. CW5 has the smallest added resistance, about 24% of the total resistance in waves, but also has the smallest wave amplitude. By comparing the results, it could be concluded that for waves of medium length in shallow water, added resistance in waves is not proportional to the square value of the wave amplitude, but that exponent becomes notably smaller.

Table 6. Added resistance in waves for all test cases

Test ID	R_{AW} , N	C_{AW}
CW2	1.39	1.35
CW3	2.94	2.85
CW5	0.32	3.50

7 CONCLUSIONS

A numerical investigation of added resistance in waves for DTC containership at model scale was carried out for two different speeds and water depths. The numerical results were validated against the experimental data and satisfactory agreement was obtained for cases with lower model speed at both 100% and 20% UKC considering that very small values were measured during the experiment. A somewhat larger relative deviation was obtained for test case with higher speed due to the numerical ventilation

that was observed on a large portion of the wetted surface area. The validation of test case CW3, which corresponds to higher model speed at 100% UKC, shows satisfactory agreement with the experimentally obtained force in the longitudinal direction. Even though numerical ventilation can be observed on a small part of the model hull in CW3 as well, it did not affect the results significantly, unlike in the case CW2 where a notable increase not only in pressure resistance but in frictional resistance as well was observed. It caused a large added resistance that is not only pressure driven, but viscous driven as well. Based on the obtained results it could be concluded that added resistance in medium waves of intermediate water depths is mostly pressure driven as in deep water as well.

8 FUTURE WORK

Plans for future work will include a verification of the numerical results by performing the analysis of grid and time step dependency. Additional steps with the respect to avoiding the occurrence of numerical ventilation will be taken in order to improve the numerical results.

9 ACKNOWLEDGEMENTS

This research was partially carried out within the framework of the Innoship project (project number 03SX416B). The authors acknowledge the financial support by the Federal Ministry for Economic Affairs and Energy (Bundesministerium für Wirtschaft und Energie) of Germany. Furthermore, the authors would like to thank the Faculty of Mechanical Engineering and Naval Architecture, University of Zagreb, for funding the licence of the software package STAR-CCM+.

10 REFERENCES

Carrica, P.M., Wilson, R. V., Noack, R.W., Stern, F., 2007. Ship motions using single-phase level set with dynamic overset grids. Comput. Fluids 36, 1415–1433. https://doi.org/10.1016/j.compfluid.2007.01.007

CD-adapco, 2018. STAR-CCM+ User Guide.

Chen, S., Hino, T., Ma, N., Gu, X., 2018. RANS investigation of influence of wave steepness on ship motions and added resistance in regular waves. J. Mar. Sci. Technol. 23, 1–13. https://doi.org/10.1007/s00773-018-0527-5

el Moctar, O., Shigunov, V., Zorn, T., 2012. Duisburg Test Case : Post-Panamax Container Ship for Benchmarking. Sh. Technol. Res. J. 59, 50–64.

Ferziger, J.H., Perić, M., 2012. Computational Methods for Fluid Dynamics. Springer Science & Business Media, Berlin.

IMO MEPC 203(62) (2011). Amendments to the annex of the protocol of 1997 to amend the international convention of pollution from ships, 1973, as modified by the protocol of 1978 relating thereto.

ITTC – Recommended Procedures and Guidelines, 2014. Practical Guidelines for Ship CFD Applications, No. 7.5–03–02–03

Kim, M., Hizir, O., Turan, O., Incecik, A., 2017. Numerical studies on added resistance and motions of KVLCC2 in head seas for various ship speeds. Ocean Eng. 140, 466–476. https://doi.org/10.1016/j.oceaneng.2017.06.019

Liu, Y., Zou, L., Zou, Z.J., Lu, T.C., Liu, J.X., 2017. Numerical Predictions of Hydrodynamic Forces and Squat of Ships in Confined Waters. Proc. 8th ICCM 1095–1110.

Quérard, A., Temarel, P., Turnock, S.R., 2008. Influence of Viscous Effects on the Hydrodynamics of Ship-Like Sections Undergoing Symmetric and Anti-Symmetric Motions, Using RANS, in: Proceedings of the ASME 27th International Conference on Offshore Mechanics and Arctic Engineering OMAE2008, June 15-20, 2008, Estoril, Portugal. pp. 683–692.

Raven, H., Van Der Ploeg, A., Starke, B., Eça, L., 2008. Towards a CFD-based prediction of ship performance.

Riesner, M., el Moctar, O., 2018. A time domain boundary element method for wave added resistance of ships taking into account viscous effects. Ocean Engineering, 162, 290-303.

Sigmund, S., el Moctar, O., 2018. Numerical and experimental investigation of added resistance of different ship types in short and long waves. Ocean Eng. 147, 51–67. https://doi.org/10.1016/j.oceaneng.2017.10.010

Tello Ruiz, M., 2018. Manoeuvring model of a container vessel in coastal waves. PhD Thesis. Ghent University.

Tello Ruiz, M., De Caluwé, S., Van Zwijnsvoorde, T., Delefortrie, G., Vantorre, M., 2015. Wave effects in 6DOF on a ship in shallow water, in: Marsim 2015. Newcastle, UK, pp. 1–15.

Tello Ruiz, M., Mansuy, M., Delefortrie, G., Vantorre, M., 2019. Modelling the manoeuvring behaviour of an ULCS in coastal waves. Ocean Eng. 172, 213–233. https://doi.org/10.1016/j.oceaneng.2018.11.046

Tello Ruiz, M., Van Hoydonck, W., Delefortrie, G., Vantorre, M., 2017. Side wall effects of ship model tests in shallow water, in: LLoys, T., van der Ploeg, A. (Eds.), 20th Numerical Towing Tank Symposium. Wageningen, The Netherlands, pp. 193–198.

Tello Ruiz, M., Vantorre, M., Delefortrie, G., 2016. Induced wave forces on a ship manoeuvring in coastal

waves. Ocean Eng. 121, 472–491.

Tezdogan, T., Demirel, Y.K., Kellett, P., Khorasanchi, M., Incecik, A., Turan, O., 2015. Full-scale unsteady RANS CFD simulations of ship behaviour and performance in head seas due to slow steaming. Ocean Eng. 97, 186–206. https://doi.org/10.1016/j.oceaneng.2015.01.011

Tezdogan, T., Incecik, A., Turan, O., 2016. Full-scale unsteady RANS simulations of vertical ship motions in shallow water. Ocean Eng. 123, 131–145. https://doi.org/10.1016/j.oceaneng.2016.06.047

Toxopeus, S.L., Simonsen, C.D., Guilmineau, E., Visonneau, M., Xing, T., Stern, F., 2013. Investigation of water depth and basin wall effects on KVLCC2 in manoeuvring motion using viscous-flow calculations. J. Mar. Sci. Technol. 18, 471–496. https://doi.org/10.1007/s00773-013-0221-6

Van Hoydonck, W., Toxopeus, S., Eloot, K., Bhawsinka, K., Queutey, P., Visonneau, M., 2018. Bank effects for KVLCC2. J. Mar. Sci. Technol. 0, 1–26. https://doi.org/10.1007/s00773-018-0545-3

Van Zwijnsvoorde, T., Tello Ruiz, M., Delefortrie, G., Lataire, E. 2019. Sailing in shallow water waves with the DTC container carrier, in: Proceedings of the 5th International Conference on Ship Manoeuvring in Shallow and Confined Water with non-exclusive focus on Manoeuvring in Waves, Wind and Current. Ostend, Belgium.

Vantorre, M., Journée, J., 2003. Validation of the strip theory code SEAWAY by model tests in very shallow water. Flanders Hydraul. Res. Numer. Model. Colloquium.

Yasukawa, H., Adnan, F.A., 2006. Experimental study on wave-induced motions and steady drift forces of an obliquely moving ship. J. Japan Soc. Nav. Archit. Ocean Eng. 3, 133–138.

11 AUTHORS BIOGRAPHY

Ivana Martić is a doctoral student of Naval Architecture and teaching/research assistant at the Faculty of Mechanical Engineering and Naval Architecture, University of Zagreb. Her area of research includes ship hydrodynamics.

Guillermo Chillcce holds the current position of research assistant at the Institute of Ship Technology, Ocean Engineering and Transport Systems (University of Duisburg-Essen). His area of expertise is seakeeping and manoeuvring analysis by means of boundary element methods and field methods.

Manases Tello Ruiz PhD, Naval Architect and Marine Engineer, is a Research Staff at Ghent University. He has been involved in several (inter)national projects with main focus on manoeuvring, seakeeping, and wave energy converters. Currently, he is working on ship air pollution and machine learning techniques applied to ship hydrodynamics. At present he is also a member of the ITTC Specialist Committee of Manoeuvring in Waves, at which he has been appointed as secretary.

Jorge Ramirez holds the current position of naval architect at Knud e Hansen in Denmark. He is responsible for performing different analyses to assist in the design process of a vessel, such as trim optimization, resistance analysis, wind loads and ship propulsion. His previous experience includes research for wave loadings on offshore wind turbines experimental and numerical analysis, wave energy converters.

Nastia Degiuli is a full professor at the Faculty of Mechanical Engineering and Naval Architecture, University of Zagreb and head of the Chair of Ship Hydrodynamics. Her area of expertise involves experimental and numerical ship hydrodynamics.

Ould el Moctar, Prof. Dr.-Ing. is full Professor in Ship Technology and Ocean Engineering at the University of Duisburg-Essen. His publications cover various aspects of hydrodynam-ics and Fluid-Structure-Interaction. The focus of his research is seakeeping, hydroelasticity, slamming and sloshing, cavitation, manoeuvring and propulsion in waves. He is editor and co-editor of many international journals.